SCIENTIFIC REPORTS

OPEN

$Au_{19}M$ (M=Cr, Mn, and Fe) as magnetic copies of the golden pyramid

Received: 8 September 2017
Accepted: 13 November 2017
Published online: 22 November 2017

Nguyen Minh Tam[1,2], Ngo Tuan Cuong[3], Hung Tan Pham[4] & Nguyen Thanh Tung[5]

An investigation on structure, stability, and magnetic properties of singly doped $Au_{19}M$ (M=Cr, Mn, and Fe) clusters is carried out by means of density functional theory calculations. The studied clusters prefer forming magnetic versions of the unique tetrahedral Au_{20}. Stable sextet $Au_{19}Cr$ is identified as the least reactive species and can be qualified as a magnetic superatom. Analysis on cluster electronic structures shows that the competition between localized and delocalized electronic states governs the stability and magnetic properties of $Au_{19}M$ clusters.

Last decades have witnessed an increasing interest in gold nano-clusters thanks to their precious catalytic, electronic, and optical properties[1–3]. In this respect, geometric and electronic structures of gold clusters with different sizes and charge states have been studied intensively through both theoretical simulations[4–8] and experiments, for instance, infrared vibrational spectroscopy[9–11], photoelectron spectroscopy[12–14], photoionization spectroscopy[15,16], photodissociation[17–19], and ion mobility measurements[20,21]. The cluster form of gold containing low-coordinated edge atoms[22] can adopt binding geometries and lead to a strong reactivity that differs from the bulk[23]. Enhanced stabilities were observed when the number of gold atoms corresponds to the following "magic" values: 2, 8, 18, 20, 34, 58, and 92, where the electronic supershells of clusters are supposed to be closed[24–29]. A rich structural diversity compared to other coinage metals has been reported for gold clusters due to their strong relativistic effects. It has been revealed that small Au_n clusters prefer planar structures till the cluster size of 8–13 atoms depending on charge states[20,30–34]. Larger species evolve via hollow cage structures at $n = 14$–18[9,35–37], tube-like structure at $n = 24$–26[38,39], fullerene type at Au_{32}[40,41], and a possibly chiral structure at $n = 34$[8]. Among the wide range of studied gold nanoclusters, the discovery of the tetrahedral Au_{20}, as an outstanding landmark in cluster science, has attracted an exceptional attention than any others[9,12,42,43]. It was reported that Au_{20} possesses a perfect pyramidal structure (T_d) with a considerably large highest occupied molecular orbital-lowest unoccupied molecular orbital (HOMO-LUMO) energy gap of 1.77 eV, suggesting its remarkably high stability and offering a potential platform for optical and catalytic nanostructured materials. The underlying physics behind its magic stability has been attributed to the formation of the 20-electron supershell closure in which each Au atom contributes one itinerant 6*s* electron[42]. Au_{20} can also be considered as either a group of ten 2-electron superatoms in superatom-network model or a superatomic molecule Au_{16} bonded with four vertex Au atoms[44].

Interests in synthesizing novel elementary units for advanced nano-structured materials led to extensive search for stable cluster species with desired properties. A presence of impurity (i.e. alkali, coinage, and transition metal) atoms can provide a key to tune the properties of Au_{20} clusters with minor effects on its magic stability. In this regard, the structures, binding energies, ionization potentials, electron affinities, and energy gaps of $Au_{19}X$ (X = Li, Na, K, Rb, Cs, Cu, and Ag) were systematically examined[45]. $Au_{19}Li$, $Au_{19}Cu$, $Au_{19}Ag$, and $Au_{19}Pt$ are found to retain the pyramidal geometry of Au_{20}[46–51]. Increasing the Ag concentration induces the energy gap and optical transition of $Au_{19-n}Ag_n$[48,49]. $Au_{19}Cu$ and $Au_{19}Pd$ clusters are potential for adsorption of trivalent arsenic[50]. Substitutional doping of Pt in Au_{20} leads to significant enhancement of the cluster binding energy and reactivity while the geometry remains the same as that of Au_{20}[51]. The 20-electron supershell closure in Au_{20} can be reproduced in a stable icosahedral $E@Au_{12}^q$ system, where E is a p-block element, through bonding-antibonding interactions between structural shells[52]. The adsorption energies of CO and O_2 on $Au_{19}H$ are similar to those on the

[1]Computational Chemistry Research Group, Ton Duc Thang University, Ho Chi Minh City, Vietnam. [2]Faculty of Applied Sciences, Ton Duc Thang University, Ho Chi Minh City, Vietnam. [3]Faculty of Chemistry and Center for Computational Science, Hanoi National University of Education, Hanoi, Vietnam. [4]Department of Chemistry, KU Leuven, Celestijnenlaan 200F, B-3001, Leuven, Belgium. [5]Institute of Materials Science and Graduate University of Science and Technology, Vietnam Academy of Science and Technology, Hanoi, Vietnam. Correspondence and requests for materials should be addressed to N.M.T. (email: nguyenminhtam@dtu.edu.vn) or N.T.T. (email: tungnt@ims.vast.ac.vn)

System	Property	This work	Other calculations[a]	Experiments[b]
Au_2	R_e	2.52	2.56	2.47
	D_e	2.27	2.14	2.29 ± 0.30
	IE	9.53	—	9.20 ± 0.21
	AE	2.08	1.82	1.92
AuCr	D_e	2.27	—	2.28 ± 0.30
	M	6		
AuMn	D_e	2.47	2.58	2.01 ± 0.22
	M	7	7	
AuFe	D_e	2.20	—	2.29 ± 0.30
Au_2Cr^+	*M*	6	—	6
Au_2Mn	*M*	6	6	—

Table 1. Theoretical and experimental results of bond length R_e (Å), dissociation energy D_e (eV), ionization energy *IE* (eV), electron affinity *EA* (eV), and spin state *M* for Au_2, AuCr, AuMn, AuFe, Au_2Cr^+, and Au_2Mn. [a]Refs[57–59]. [b]Refs[60–62].

Au_{20} cluster[53]. More recently, selective doping with Hf and Ge atoms has been applied to modify the catalytic activity of Au_{20} through transforming the cluster structure[54].

Although there have been some progress on the structural features and catalytic behavior of doped 20-atom gold clusters, the role of impurities in tailoring the magnetic properties of Au_{20} has been far less understood. Considering the fact that Cr, Mn, and Fe are interesting magnetic elements due to their unpaired $4s^13d^5$, $4s^23d^5$, and $4s^23d^6$ valence electrons, respectively, the interaction between these impurities and host electrons is expected to trigger essential changes in the magnetism of 20-atom gold clusters. In this study, we report results on searching for lowest-lying structures of gold clusters doped with a transition metal impurity $Au_{19}M$ (M=Cr, Mn, and Fe) and discussing the origin of their magnetic and stability properties. The finding results unravel the possibility of producing new magnetic superatoms in the golden pyramid's family.

Computational setup

The structural optimization of $Au_{19}M$ clusters have been carried out by density functional theory (DFT) calculations implemented in the Gaussian 09 software[55,56]. We used the BP86 functional in conjunction with basis sets cc-pvDZ-pp for Au and cc-pvDZ for Cr, Mn, and Fe. Possible structures of $Au_{19}M$ clusters were generated using a stochastic algorithm[57]. In addition, the local minima of previously-reported doped Au_n clusters also served as reference input. All guessing structures were initially optimized using the BP86 functional in jointing with cc-pvDZ-pp for Au atoms and cc-pvDZ for Cr, Mn and Fe dopants. Isomers having relative energies within 2.0 eV were selected for recalculating single point energies at the same functional but combining with larger basis set, cc-pvTZ-pp for Au and cc-pvTZ for Cr, Mn, and Fe. In the following, we discuss the structural, stability, and magnetic aspects of the doped $Au_{19}M$ clusters.

The selection of the BP86/cc-pvDZ-pp and cc-pvDZ functional resulted from test calculations for Au_2, AuCr, AuMn, AuFe, Au_2Cr^+, and Au_2Mn. The calculated results are presented in Table 1, along with available computational and experimental data for comparison. It can be seen that the used level provide reliable results for all of the examined properties. For example, the calculated spin states of all dimers and molecules are in excellent agreement with the other theoretical and experimental values[58–63]. The computed D_e of Au_2, AuCr, and AuFe are 2.27, 2.27, and 2.20 eV, which are well consistent with the experimental ones, 2.29 ± 0.30, 2.28 ± 0.30, and 2.29 ± 0.30 eV, respectively. Although the predicted D_e of AuMn obtained in this work likely overestimates the experimental one, it is apparently in closer agreement with experiment than that of other calculations. It is worth to mention that the BP86 functional has been proved to yield the most reliable results for yttrium and vanadium doped gold species[64–66]. Therefore we are confident that the used computational approach is suitable to describe the structures and properties of $Au_{19}M$ clusters.

Results and Discussions

The geometries of low-lying $Au_{19}M$ isomers with M=Au, Cr, Mn, and Fe are shown in Fig. 1. Although a large number of different structures and spin configurations are considered for each cluster, only the lowest-energy isomers are discussed. As expected, singlet Au_{20} is found to be very stable in form of a tetrahedral with a calculated HOMO-LUMO energy gap of 1.80 eV, in an excellent agreement with the measured value (1.77 eV)[12]. It is noteworthy that the ground-state geometry of all investigated clusters favor a slightly distorted tetrahedral form caused by the displacement of the impurity, where the dopant substitutes for a gold atom on the surface center. The second lower-lying isomers of $Au_{19}Cr$, $Au_{19}Mn$, and $Au_{19}Fe$ have the same motif of an endohedrally-doped truncated pyramid, lying at 0.33, 0.08, and 0.23 eV above their corresponding ground states, respectively. A tetrahedron with a substituted dopant atom on the edge serves as the next isomers of $Au_{19}Cr$ and $Au_{19}Fe$ with relative energies of 0.48 and 0.29 eV, respectively. On the other side, that of $Au_{19}Mn$ is a spin isomer (septet) of the corresponding ground state, locating at 0.14 eV higher in energy.

The most interesting feature of $Au_{19}M$ clusters is their magnetic behavior. Unlike the non-magnetic Au_{20}, the ground state spin multiplicities of $Au_{19}Cr$, $Au_{19}Mn$, and $Au_{19}Fe$ clusters are sextet, quintet, and quartet, corresponding to total magnetic moments of 5, 4, and 3 μ_B, respectively. The decreasing trend of the total magnetic

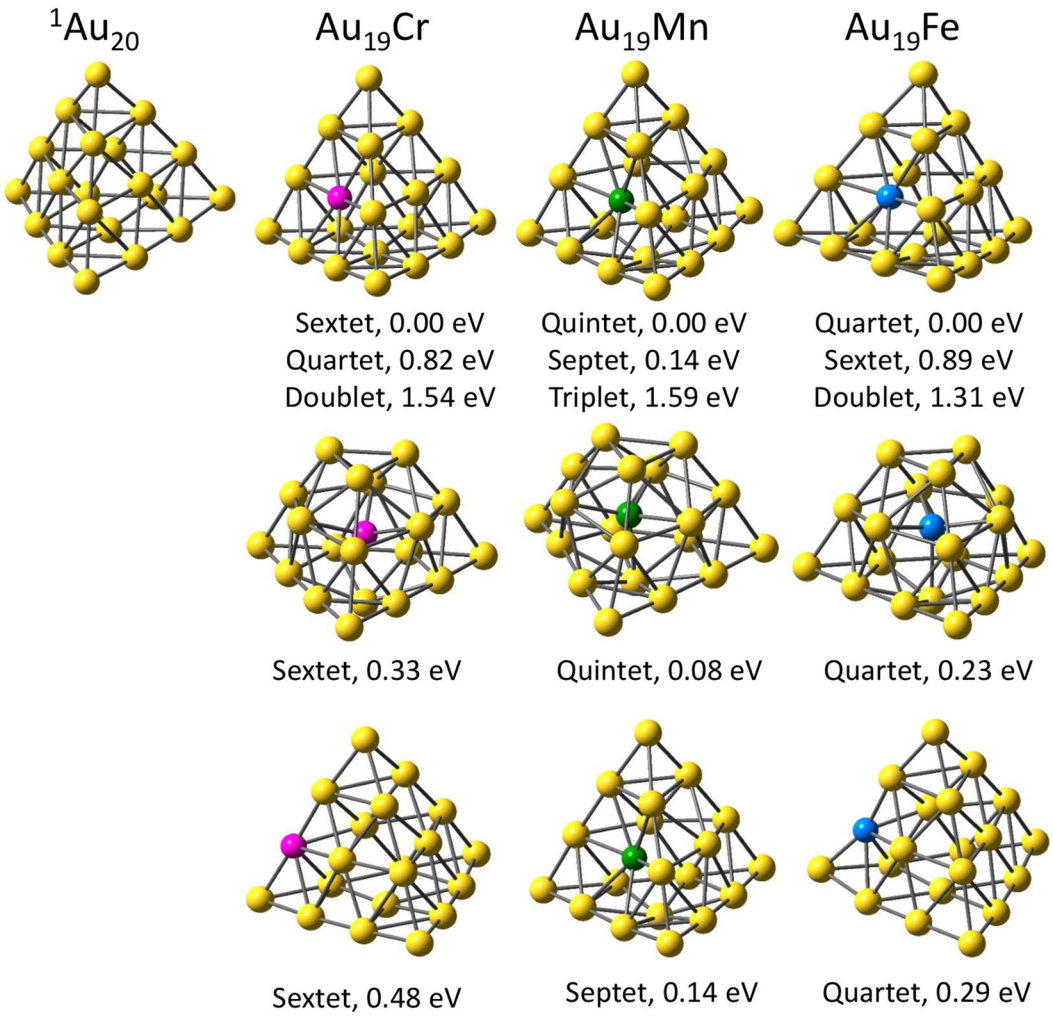

Figure 1. Optimized shapes and lowest-lying spin multiplicities of $Au_{19}M$ (M=Cr, Mn, and Fe) clusters with relative energies. The yellow, purple, green, and blue spheres represent Au, Cr, Mn, and Fe atoms, respectively.

moments with the increasing number of dopant's valence electrons is noticeable. Other low-lying spin isomers are examined and listed in Fig. 1. It is found that the ground states of Cr and Fe doped Au_{19} clusters have relatively robust spin configurations. In particular, the next spin excitations of $Au_{19}Cr$ are quartet and doublet at 0.82 and 1.54 eV, respectively. For $Au_{19}Fe$, at least 0.89 eV is needed to excite it from quartet to sextet states and 1.31 eV is required for the quartet-to-doublet transition. The spin stability of $Au_{19}Cr$ and $Au_{19}Fe$ is again reflected by the fact that their second and third lowest-energy isomers also favor the same spin states as the ground state ones. Whereas, the spin ground state of $Au_{19}Mn$ is less stable since an energy amount of 0.14 eV is sufficient to trigger a spin excitation.

To gain insight into the magnetic behavior of $Au_{19}M$ clusters, the total/partial density of states (DOS), the molecular orbitals (MO) diagram, and the spin distribution of $Au_{19}M$ clusters are calculated and plotted in Fig. 2. Typically, when a metallic cluster is doped with a magnetic atom, the outermost orbitals of the magnetic impurity can hybridize with delocalized orbitals of the host to form supershells. Cr, Mn, and Fe atoms have electronic configurations of $[Ar]4s^13d^5$, $[Ar]4s^23d^5$, and $[Ar]4s^23d^6$ corresponding to 6, 7, and 8 valence electrons, respectively. Assuming the each gold atom delocalizes one 6*s* electron, adding a Cr atom to the cluster of nineteenth gold atoms can create a pool of 25 itinerant electrons. Ordinarily, this forms an open shell of $2P^5$ and does not lead to the observed spin state. However, there is another possibility in which valence orbitals of the Cr atom and delocalized MOs of the host hybridize and form a localized and a delocalized MO sets[67]. Once the delocalized MO set occupies states of itinerant electrons, the localized MO set has enough exchange splitting to cause a magnetic moment. With this picture in mind, the first 20 delocalized electrons of a $Au_{19}Cr$ cluster might be used to fill the molecular shell of $1S^21P^62S^21D^{10}$, which leads to the stable species. Its five remaining localized electrons are taken to partially fill the *d*-Cr atomic shell, which results in a total magnetic moment of 5 μ_B. Similar argument can be applied for $Au_{19}Mn$ and $Au_{19}Fe$, in which their delocalized electrons fulfill a shell configuration of $1S^21P^62S^21D^{10}$ and magnetic moments oscillates between 4 and 3 μ_B, depending on the number of valence electrons in dopant atoms.

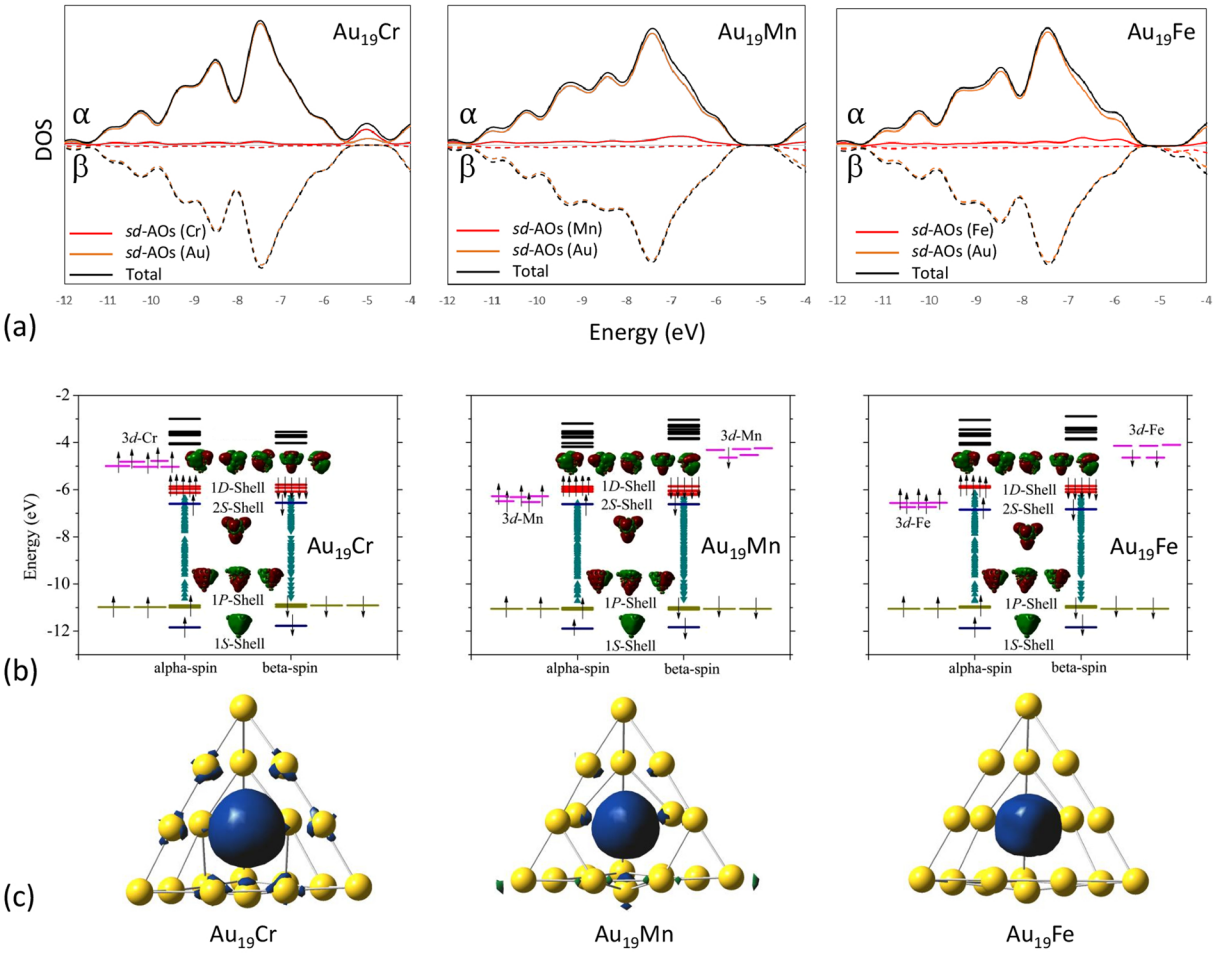

Figure 2. (**a**) Partial and total density of electronic states (DOS) and (**b**) one-electron-energy-level molecular diagrams (MO) of $Au_{19}M$ clusters. The black lines represent energy levels of the lowest unoccupied molecular orbitals (LUMO). The red, blue, dark yellow, and navy lines depict orbitals corresponding to the 1D, 2S, 1P, and 1S supershells, respectively. The magenta lines describe the localized 3*d*-M orbitals. The light blue triangles correspond for filled *d*-orbitals of Au atoms, which do not contribute to the supershell. Each upward (or downward) arrow represents one alpha-spin (or beta-spin) electron. (**c**) Total spin distribution of $Au_{19}M$ clusters plotted at a density of 0.004. The navy basins are for alpha-spin while the green ones are for beta-spin.

The results presented in Fig. 2 confirm the latter picture. The total/partial DOS [Fig. 2(a)] in combination with the MO diagram [Fig. 2(b)] indicate that the *s* orbitals from Au atoms play an essential role to the cluster shell orbitals while the half-filled *sd* orbitals of transition metal dopants become a key factor for the magnetic moment of studied species. In particular, the hybridized *sd*-M and *s*-Au electrons in $Au_{19}M$ clusters form both localized and delocalized electronic states. Similar to Au_{20}, the delocalized states can be expressed in the full occupied electron shell sequence of $1S^21P^62S^21D^{10}$. Two low-energy DOS peaks at −11.9 and −11.0 eV response for the molecular shell orbitals 1*S* and 1*P* (navy and dark yellow levels), respectively. The molecular shell orbitals 2*S* and 1*D* (blue and red levels) that overlap with atomic orbitals *d* of Au atoms (light blue levels) are observed at −6.5 and 6.0 eV, respectively. Meanwhile, the localized states (magenta levels) are used to fill the atomic five *d* orbitals from the dopant atom with five, six, and seven electrons from $Au_{19}Cr$, $Au_{19}Mn$, and $Au_{19}Fe$ clusters, respectively. Since the delocalized states account for the 20-electron supershell closure, the unpaired electrons in the localized *d* orbitals cause the magnetic moments of clusters. It can be approximately considered that the chromium atom provides one electron to the cluster supershells and five others to the majority spin channel of *d* atomic subshell orbitals. Similarly, the manganese (iron) atom donates one electron to the cluster supershell orbitals, five electrons to the majority spin channel, and one (two) other(s) to the minority spin channel, respectively. According to the energy levels in MO diagrams, the electronic configurations of $Au_{19}Cr$, $Au_{19}Mn$, and $Au_{19}Fe$ clusters can be written as $1S^21P^62S^23d_{\uparrow}^{5}1D^{10}$, $1S^21P^62S^23d_{\uparrow}^{5}1D^{10}3d_{\downarrow}^{1}$, and $1S^21P^62S^23d_{\uparrow}^{5}1D^{10}3d_{\downarrow}^{2}$, respectively. This picture can be further examined by mapping the spin distribution of studied $Au_{19}M$ clusters. As shown in Fig. 2(c), the total spin of the clusters is largely localized at the dopant atom, provided by the 3*d* state electrons as described in their aforementioned electronic configurations. A small amount of ferrimagnetic spin alignment adding to the total magnetic moments is found in Au atoms. Calculated local magnetic moments of $Au_{19}M$ clusters (not shown here)

Clusters	$\varepsilon_{HOMO}^{alpha}$	$\varepsilon_{LUMO}^{alpha}$	$\varepsilon_{HOMO}^{beta}$	$\varepsilon_{LUMO}^{beta}$	δ_1	δ_2
$Au_{19}Cr$	−4.83	−4.06	−5.79	−4.05	0.78	1.73
$Au_{19}Mn$	−5.86	−4.18	−4.44	−4.31	1.55	0.26
$Au_{19}Fe$	−5.84	−4.08	−4.66	−4.10	1.74	0.58

Table 2. Calculated HOMO and LUMO energies (in eV) of the majority and minority spin channels and the values (in eV) of δ_1 and δ_2 for $Au_{19}M$ (M=Cr, Mn, and Fe).

supports our argument that the total magnetic moments in $Au_{19}M$ clusters essentially result from the localized 3*d*-M orbitals.

Inheriting the major 20-electron supershell closing $1S^21P^62S^21D^{10}$ and highly symmetric geometry from the tetrahedral Au_{20}, $Au_{19}Cr$, $Au_{19}Mn$, and $Au_{19}Fe$ are potentially stable species. Their dopant-dependent stability can be reflected through the comparison between corresponding binding energies per atom E_b with that of Au_{20}. The calculated average binding energy of Au_{20} is found as 2.25 eV, which is in good agreement with the previously reported values[58]. Whereas, E_b of alloy species are slightly higher, that are 2.29, 2.30, and 2.31 eV for $Au_{19}Cr$, $Au_{19}Mn$, and $Au_{19}Fe$ clusters, respectively. Since the $Au_{19}M$ and Au_{20} systems have nearly identical geometries and similar E_b values, it could be suggested that the incorporation of transition metal dopants tends to stabilize the gold host and the stability of $Au_{19}M$ system can be relatively comparable to that of the robust Au_{20}. We further examine the bonding nature between the dopant and Au host by analyzing the electron localizability indicator (ELI-D)[68]. The ELI-D isosurface of $Au_{19}M$ clusters produced at the bifurcation value of 1.0 are presented in Fig. S1 in the Supplementary Information file (Supplementary Information: The electron localizability of ground-state $Au_{19}M$ clusters). No localization domain is observed in the region between the dopant and Au_{19} host, implying that the dopant likely connects with Au moiety via ionic and/or highly polarized covalent bonds. A similar picture was also reported for $Re@Au_{11}Pt$ and $Ta@Au_{11}Hg$ superatomic systems, in which the energy decomposition analysis (ETS-NOCV) is used to emphasizes the importance of electrostatic and covalent interaction between metal dopant and host in stabilizing clusters[69]. To measure the chemical stability of the clusters, we examine the energy gaps between the LUMO of the minority (beta) spin and the HOMO of the majority (alpha) spin $[\delta_1 = -(\varepsilon_{HOMO}^{alpha} - \varepsilon_{LUMO}^{beta})]$ and between the LUMO of the majority (alpha) spin and the HOMO of the minority (beta) spin $[\delta_2 = -(\varepsilon_{HOMO}^{beta} - \varepsilon_{LUMO}^{alpha})]$. These values suggest the required amount of energy for an electron to jump from the HOMO of majority (minority) spin channel to the LUMO of minority (majority) one. The larger gap means the less reactive and more stable clusters[70–72]. Table 2 lists the HOMO and LUMO energies for the majority and minority spin channels and the values of δ_1 and δ_2 calculated for the ground states. Both energy gaps δ_1 and δ_2 take positive values, again confirming the inertness of all studied clusters. Notably, $Au_{19}Cr$ has the largest gaps of δ_1 and δ_2, which means that it is the most stable and least reactive species compared to the others and can be assigned as a magnetic superatom. Among clusters with higher doping concentration, $Au_{16}M_4$ would be a promising system due to its potential as a giant magnetic and highly symmetric superatom. Although the dopant atom apparently prefers substituting one Au atom in the surface center of singly doped species, the situation for $Au_{16}M_4$ clusters could be more puzzling. It is worth to mention that the unique stability of the golden pyramid Au_{20} can be understood in term of a superatomic molecule $Au_{16}Au_4$, where its superatomic core Au_{16} binds with four vertex Au atoms[42]. This approach has been supported by the recent findings of the golden pyramid's smaller sisters, the tetrahedral Au_{17}^+ and Au_{10}^{2+}. These two systems were found highly stable in form of Au_{13} and Au_6 octahedral cores, respectively, and the other four gold atoms are above four their triangular faces[37,73,74]. In this scenario, $Au_{16}M_4$ and its smaller magnetic counterparts, $Au_{13}M_4^+$ and $Au_6M_4^{2+}$, might be considered as a core in −4 charge state and four vertex M atoms. A careful examination of this interesting issue is perhaps warranted for future research.

Conclusions

In summary, we have investigated structure, stability, and magnetic properties of singly doped $Au_{19}M$ (M=Cr, Mn, and Fe) clusters using DFT calculations. The most interesting point of our results is that all studied $Au_{19}M$ clusters favorably form magnetic copies of the golden pyramid Au_{20}. The dopant atom is found to substitute for a gold atom on the surface center. The coexistence of both delocalized and localized electronic states in these clusters allows to fill the supershell orbitals and to simultaneously promote local magnetic moments, leading to stable magnetic systems. $Au_{19}Cr$ is the most stable species that can be assigned as a magnetic sister of the golden pyramid Au_{20}.

References

1. Haruta, M. Size- and support-dependency in the catalysis of gold. *Catal. Today* **36**, 153–166 (1997).
2. Daniel, M. C. & Astruc, D. Gold nanoparticles: Assembly, supramolecular chemistry, quantum-size-related properties, and applications toward biology, Catalysis, and Nanotechnology. *Chem. Rev.* **104**, 293–346 (2004).
3. Pyykkö, P. Structural properties: Magic nanoclusters of gold. *Nat. Nanotechnol.* **2**, 273–274 (2007).
4. Häberlen, O. D., Schmidbauer, H. & Rösch, N. Stability of main-group element-centered gold cluster cations. *J. Am. Chem. Soc.* **116**, 8241–8248 (1994).
5. Häkkinen, H. & Landman, U. Gold clusters (Au_N, $2 < N < 10$) and their anions. *Phy. Rev. B* **62**, R2287 (2000).
6. Zhang, Z., Berg, A., Levanon, H., Fessenden, R. & Meisel, W. D. On the interactions of free radicals with gold nanoparticles. *J. Am. Chem. Soc.* **125**, 7959–7963 (2003).
7. Chen, M. S. & Goodman, D. W. The structure of catalytically active gold on titania. *Science* **306**, 252–255 (2004).
8. Lechtken, A. *et al.* Au_{34}^-: A chiral gold cluster? *Angew. Chem., Int. Ed.* **46**, 2944–2948 (2007).
9. Gruene, P. *et al.* Structures of neutral Au_7, Au_{19}, and Au_{20} clusters in the gas phase. *Science* **321**, 674–676 (2008).

10. Ghiringhelli, L. M. *et al*. Not so loosely bound rare gas atoms: finite-temperature vibrational fingerprints of neutral gold-cluster complexes. *New J. Phys.* **15**, 083003 (2013).
11. Yang, Z., León, I. & Wang, L. S. Vibrational spectroscopy of Au_4 from high resolution photoelectron imaging. *J. Chem. Phys.* **139**, 021106 (2013).
12. Li, J., Li, X., Zhai, H. J. & Wang, L. S. Au_{20}: a tetrahedral cluster. *Science* **299**, 864–867 (2003).
13. Wang, L. M. & Wang, L. S. Probing the electronic properties and structural evolution of anionic gold clusters in the gas phase. *Nanoscale* **4**, 4038–4053 (2012).
14. León, I., Yang, Z. & Wang, L. S. High resolution photoelectron imaging of Au_3^-. *J. Chem. Phys.* **138**, 184304 (2013).
15. Jackschath, C., Rabin, I. & Schulze, W. Electronic Structures and related properties. Electron impact ionization potentials of gold and silver clusters Me_n, $n \leq 22$. *Ber. Bunsenges. Phys. Chem.* **96**, 1200–1204 (1992).
16. Bishea, G. A. & Morse, M. D. Resonant two-photon ionization spectroscopy of jet-cooled Au_3. *J. Chem. Phys.* **95**, 8779 (1991).
17. Vogel, M., Hansen, K., Herlert, A. & Schweikhard, L. Decay pathways of small gold clusters. *Eur. Phys. J. D* **16**, 73–76 (2001).
18. Hansen, K., Herlert, A., Schweikhard, L. & Vogel, M. Dissociation energies of gold clusters Au_N^+, $N = 7$–27. *Phys. Rev. A* **73**, 063202 (2006).
19. Veldeman, N. *et al*. Stability and dissociation pathways of doped Au_nX^+ clusters (X = Y, Er, Nb). *Faraday Discuss.* **138**, 147–162 (2008).
20. Gilb, S., Weis, P., Furche, F., Ahlrichs, R. & Kappes, M. M. Structures of small gold cluster cations (Au_n^+, $n < 14$): Ion mobility measurements versus density functional calculations. *J. Chem. Phys* **116**, 4094 (2002).
21. Furche, F. *et al*. The structures of small gold cluster anions as determined by a combination of ion mobility measurements and density functional calculations. *J. Chem. Phys.* **117**, 6982 (2002).
22. Lemire, C., Meyer, R., Shaikhutdinov, S. & Freund, H. J. Do quantum size effects control CO adsorption on gold nanoparticles? *Angew. Chem. Int. Ed.* **43**, 118 (2004).
23. Mills, G., Gordon, M. S. & Metiu, H. Oxygen adsorption on Au clusters and a rough Au(111) surface: The role of surface flatness, electron confinement, excess electrons, and band gap. *J. Chem. Phys.* **118**, 4198 (2003).
24. Walter, M. *et al*. A unified view of ligand-protected gold clusters as superatom complexes. *Proc. Natl. Acad. Sci. USA* **105**, 9157–9162 (2008).
25. Jadzinsky, P., Calero, G., Ackerson, C., Bushnell, D. & Kornberg, R. Structure of a thiol monolayer-protected gold nanoparticle at 1.1 Å resolution. *Science* **318**, 430–433 (2007).
26. Dass, A. Mass spectrometric identification of $Au_{68}(SR)_{34}$ molecular gold nanoclusters with 34-electron shell closing. *J. Am. Chem. Soc.* **131**, 11666 (2009).
27. Price, R. & Whetten, R. All-aromatic, nanometer-scale, gold-cluster thiolate complexes. *J. Am. Chem. Soc.* **127**, 13750 (2005).
28. Heaven, M., Dass, A., White, P., Holt, K. & Murray, R. Crystal structure of the gold nanoparticle $[N(C_8H_{17})_4]$ $[Au_{25}(SCH_2CH_2Ph)_{18}]$. *J. Am. Chem. Soc.* **130**, 3754 (2008).
29. Zhang, Y. *et al*. Application of HPLC and MALDI-TOF MS for studying as-synthesized ligand-protected gold nanoclusters products. *Anal. Chem.* **81**, 1676–1685 (2009).
30. Mills, G., Gordon, M. & Metiu, H. The adsorption of molecular oxygen on neutral and negative Au_n clusters ($n = 2$–5). *Chem. Phys. Lett.* **359**, 493–499 (2002).
31. Pyykkö, P. Theoretical chemistry of gold. III. *Chem. Soc. Rev.* **37**, 1967–1997 (2008).
32. Olson, R. *et al*. Where does the planar-to-nonplanar turnover occur in small gold clusters? *J. Am. Chem. Soc.* **127**, 1049–1052 (2005).
33. Spivey, K., Williams, J. & Wang, L. Structures of undecagold clusters: Ligand effect. *Chem. Phys. Lett.* **432**, 163–166 (2006).
34. Gruber, M., Heimel, G., Romaner, L., Bredas, J. L. & Zojer, E. First-principles study of the geometric and electronic structure of Au_{13} clusters: Importance of the prism motif. *Phys. Rev. B* **77**, 165411 (2008).
35. Bulusu, S. & Zeng, X. Structures and relative stability of neutral gold clusters: Au_n ($n = 15$–19). *J. Chem. Phys.* **125**, 154303 (2006).
36. Gao, Y., Shao, N., Pei, Y., Chen, Z. & Zeng, X. Catalytic activities of subnanometer gold clusters (Au_{16}-Au_{18}, Au_{20}, and Au_{27}-Au_{35}) for CO oxidation. *ACS Nano* **5**, 7818–7829 (2011).
37. Yan, L., Cheng, L. & Yang, J. Tetrahedral Au_{17}^+: A superatomic molecule with a Au_{13} FCC core. *J. Chem. Phys. C* **119**, 23274–23278 (2015).
38. Fa, W. & Dong, J. Possible ground-state structure of Au_{26}: A highly symmetric tubelike cage. *J. Chem. Phys.* **124**, 114310 (2006).
39. Xing, X., Yoon, B., Landman, U. & Parks, J. H. Structural evolution of Au nanoclusters: From planar to cage to tubular motifs. *Phys. Rev. B* **74**, 165423 (2006).
40. Johansson, M., Sundholm, D. & Vaara, J. Au_{32}: A 24-carat golden fullerene. *Angew. Chem., Int. Ed.* **43**, 2678 (2004).
41. Gu, X., Ji, M., Wei, S. H. & Gong, X. G. Au_N clusters ($N = 32, 33, 34, 35$): Cagelike structures of pure metal atoms. *Phys. Rev. B* **70**, 205401 (2004).
42. Cheng, L., Zhang, X., Jin, B. & Yang, J. Superatom-atom super-bonding in metallic clusters: a new look to the mystery of an Au_{20} pyramid. *Nanoscale* **6**, 12440 (2014).
43. Huang, W., Bulusu, S., Pal, R., Zeng, X. C. & Wang, L. S. Structural transition of gold nanoclusters: From the golden cage to the golden pyramid. *ACS Nano* **3**, 1225–1230 (2009).
44. Muñoz-Castro, A. & King, R. B. Au_{20}. Effect of a strong tetrahedral field in a spherical concentric bonding shell model. *J. Phys. Chem. C* **121**, 5848 (2017).
45. Ghanty, T. K., Banerjee, A. & Chakrabarti, A. Structures and the electronic properties of $Au_{19}X$ clusters (X = Li, Na, K, Rb, Cs, Cu, and Ag). *J. Phys. Chem. C* **114**, 20 (2010).
46. Mondal, K., Ghanty, T. K., Banerjee, A., Chakrabarti, A. & Kamal, C. Density functional investigation on the structures and properties of Li atom doped Au_{20} cluster. *Mol. Phys.* **111**, 725–734 (2013).
47. Mondal, K., Manna, D., Ghanty, T. K. & Banerjee, A. Significant modulation of CO adsorption on bimetallic $Au_{19}Li$ cluster. *Chem. Phys.* **428**, 75–81 (2014).
48. Zhang, X. D. *et al*. First-principles investigation of Ag-doped gold nanoclusters. *Int. J. Mol. Sci.* **12**, 2972–2981 (2011).
49. Polynskaya, Y. G., Pichugina, D. A. & Kuz'menko, N. E. Correlation between electronic properties and reactivity toward oxygen of tetrahedral gold-silver clusters. *Comput. Theor. Chem.* **1055**, 61–67 (2015).
50. Arriagada, D. C. & Toro, E. A. Insights into the use of $Au_{19}Cu$ and $Au_{19}Pd$ clusters for adsorption of trivalent arsenic. *Theor. Chem. Acc.* **135**, 52 (2016).
51. Mondal, K., Banerjee, A. & Ghanty, T. K. Structural and chemical properties of subnanometer-sized bimetallic $Au_{19}Pt$ cluster. *J. Phys. Chem. C* **118**, 11935 (2014).
52. Muñoz-Castro, A. Golden endohedral main-group clusters, $[E@Au_{12}]^{q-}$: Theoretical insights into the 20-e principle. *J. Phys. Chem. Lett.* **4**, 3363 (2013).
53. Mondal, K., Agrawal, S., Manna, D., Banerjee, A. & Ghanty, T. K. Effect of hydrogen atom doping on the structure and electronic properties of 20-atom gold cluster. *J. Phys. Chem. C* **120**, 18588 (2016).
54. Manzoor, D., Krishnamurty, S. & Pal, S. Contriving a catalytically active structure from an inert conformation: A density functional investigation of Al, Hf, and Ge doping of Au_{20} tetrahedral clusters. *J. Phys. Chem. C* **120**, 19636 (2016).
55. Frisch, M. J. *et al*. Gaussian 09, Revision A.02 (Gaussian, Inc., Wallingford CT, 2009).
56. Hohenberg, P. & Kohn, W. Inhomogeneous electron gas. *Phys. Rev.* **136**, B864 (1964).

57. Pham, H. T., Long, D. V., Pham, B. Q. & Nguyen, M. T. The 2D-to-3D geometry hopping in small boron clusters: The charge effect. *Chem. Phys. Lett.* **577**, 32–37 (2013).
58. Idrobo, J. C. *et al*. Static polarizabilities and optical absorption spectra of gold clusters (Au_n, $n = 2$–14 and 20) from first principles. *Phys. Rev. B* **76**, 205422 (2007).
59. Dong, D., Xiao-Yub, K., Jian-Juna, G. & Ben-Xia, Z. Geometries, stabilities, and magnetic properties of $CrAu_n$ ($n = 1$–8) clusters: Density functional theory study. *Physica A* **389**, 5216 (2010).
60. Zhang, M., Zhang, H., Zhao, L., Li, Y. & Luo, Y. Low-energy isomer identification, structural evolution, and magnetic properties in manganese-doped gold clusters $MnAu_n$ ($n = 1$–16). *J. Phys. Chem. A* **116**, 1493 (2012).
61. Morse, M. D. Clusters of transition-metal atoms. *Chem. Rev.* **86**, 1079 (1986).
62. Jackslath, C., Rabin, I. & Schulze, W. Electronic structures and related properties. Electron impact ionization potentials of gold and silver clusters Me_n, $n = 22$. *Ber. Bunsenges. Phys. Chem.* **96**, 1200 (1992).
63. Häkkinen, H. *et al*. On the electronic and atomic structures of small Au_N^- ($N = 4$–14) clusters: A photoelectron spectroscopy and density-functional study. *J. Phys. Chem. A* **107**, 6168 (2003).
64. Lin, L. *et al*. Fluxionality and σ-aromaticity in small yttrium-doped gold clusters. *ChemPhysChem* **9**, 2471–2474 (2008).
65. Lin, L. *et al*. Far-infrared spectra of yttrium-doped gold clusters Au_nY ($n = 1$–9). *ChemPhysChem* **11**, 1932–1943 (2010).
66. Nhat, P. V. & Nguyen, M. T. Trends in structural, electronic and energetic properties of bimetallic vanadium-gold clusters Au_nV with $n = 1$–14. *Phys. Chem. Chem. Phys* **13**, 16254–16264 (2011).
67. Reveles, J. U. *et al*. Designer magnetic superatoms. *Nature Chem.* **1**, 310–315 (2009).
68. Kohout, M., Wanger, F. R. & Grin, Y. Atomic shells from the electron localizability in momentum space. *Int. J. Quantum Chem.* **106**, 1499 (2006).
69. Muñoz-Castro, A. Doping the cage. $Re@Au_{11}Pt$ and $Ta@Au_{11}Hg$, as novel 18-ve trimetallic superatoms displaying a doped icosahedral golden cage. *Phys. Chem. Chem. Phys.* **19**, 2453 (2017).
70. Wang, Q., Sun, Q., Briere, T. M. & Kawazoe, Y. First-principles study of the magic Ar_6Fe^+ cluster. *Mater. Trans.* **42**, 2172–2174 (2001).
71. Datta, S., Kabir, M., Saha-Dasgupta, T. & Mookerjee, A. Structure, reactivity, and electronic properties of V-doped Co clusters. *Phys. Rev. B* **80**, 085418 (2009).
72. Venkataramanan, N. S., Sahara, R., Mizuseki, H. & Kawazoe, Y. Titanium-doped nickel clusters $TiNi_n$ ($n = 1$–12): Geometry, electronic, magnetic, and hydrogen adsorption properties. *J. Phys. Chem. A* **114**, 5049–5057 (2010).
73. Petrar, P. M., Sárosi, M. B. & King, R. B. Au_{10}^{2+}: A tetrahedral cluster exhibiting spherical aromaticity. *J. Phys. Chem. Lett.* **3**, 3335 (2012).
74. Muñoz-Castro, A. Au_{10}^{2+} and $Au_6X_4^{2+}$ clusters: Superatomic molecules bearing an SP^3-hybrid Au_6 core. *Int. J. Quantum Chem.* **117**, 25331 (2017).

Acknowledgements

N.T.T. acknowledges support by the National Key Laboratory of Electronic Materials and Devices and the Institute of Materials Science, Vietnam Academy of Science and Technology under grant number CSCL05.2017. N.T.C. thanks the Ministry of Education and Training of Vietnam for financial support under grant number B2015-17-68.

Author Contributions

N.M.T. and N.T.T. conceived the calculations, N.M.T. and H.P.T. conducted the calculations, N.T.C. and N.T.T. analysed the results. All authors prepared and reviewed the manuscript.

Additional Information

Supplementary information accompanies this paper at https://doi.org/10.1038/s41598-017-16412-3.

Competing Interests: The authors declare that they have no competing interests.

Publisher's note: Springer Nature remains neutral with regard to jurisdictional claims in published maps and institutional affiliations.